# Efficient Adsorption of Four Phenolic Compounds using a Robust Nanocomposite Fabricated by Confining 2D Porous Organic Polymers in 3D Anion Exchangers

Zhen Yang,[*a] Yi Zhang,[a] Xuzeng Wang,[a] Ziqi Tian,[c] Weiben Yang,[*a] and Nigel J. D. Graham[*b]

[a] School of Chemistry and Materials Science, Jiangsu Provincial Key Laboratory of Material Cycling and Pollution Control, Nanjing Normal University, Nanjing 210046, China

[b] Department of Civil and Environmental Engineering, Imperial College London, SW7 2AZ, UK

[c] Ningbo Institute of Materials Technology & Engineering, Chinese Academy of Sciences, Ningbo 315000, China

[*] Corresponding authors.

All authors' email address: yangzhen@njnu.edu.cn (Z. Yang); 793724568@qq.com (Y. Zhang); 517719855@qq.com (X.Z. Wang); tianziqi@nimte.ac.cn (Z.Q. Tian); yangwb007@njnu.edu.cn (W.B. Yang); n.graham@imperial.ac.uk (N.J.D. Graham)

**Abstract:** A novel 2D/3D hybrid nanocomposite adsorbent (TCBD/D318) was synthesized by confining 2D porous organic polymers (POP, TCBD) in pores of commercial 3D anionic exchanger beads (D318) using a facile repetitive deposition method, and evaluated for the removal of four phenolic contaminants (phenol, 1-naphthol, 4-nitrophenol and 4-chlorophenol) from water. The immobilization of TCBD in D318 conferred on the adsorbent a robust water stability, a rapid solid-liquid separation (in 10 s after dispersion in water), and an enhanced anti-self-aggregation property. The effects of pH, contaminant type, coexisting inorganic anions and natural organic matter (NOM) on adsorption performance were studied. TCBD/D318 exhibited high adsorption capacities ($Q_e$) for all four phenolic contaminants, and these were only slightly influenced by pH and the presence of coexisting inorganic anions and NOM, due to the combined effects of multi-binding-interactions and hierarchical pore-structures. Another equally important merit of the TCBD/D318 was its remarkably improved utilization efficiency (atom economy) of functional groups. The adsorption mechanisms were investigated by a combination of physico-chemical model fitting, instrumental analysis and chemical computation. These displayed a hierarchical-pore-structure-induced multi-step diffusion adsorption involving multi-binding-interactions, principally electrostatic attraction, π-π interaction, and H-bonding; the contaminants were more inclined to be bound onto TC units of TCBD in the nanocomposite. Regeneration tests involving 10 adsorption-desorption cycles showed that TCBD/D318 maintained a high $Q_e$, confirming its effective reusability. The results have demonstrated the outstanding potential of TCBD/D318 for the removal of phenolic compounds from water, and more generally the possibilities of using POP-based 2D/3D hybrid nanocomposites in wider environmental applications.

**Keywords:** Adsorption; Phenolic contaminants; Porous organic polymers; Anion

exchange resin; Nanocomposite

## 1. Introduction

In many countries throughout the world the provision of clean and safe drinking water is an increasing problem owing to the deterioration of natural water sources [1]. In particular, phenolic contaminants, mainly originating from industrial, agricultural and domestic activities, pose serious hazards to the water environment [2]. These contaminants have attracted continuous attention over many decades; for example, the World Health Organization proposed a maximum admissible concentration (MAC) for phenolic substances in drinking water in 1958 [3], and the US Environmental Protection Agency (EPA) assigned a MAC range-toxicity relationship in 1984 [4]. However, their removal from contaminated waters still remains important (especially in developing countries with rapid expansion of industries related to these compounds), considering their direct human-life-threat [5], linkages to carcinogenic disinfection-by-products [6], and production of unpleasant tastes and odour in water [7].

Adsorption is a facile, effective and reliable separation method among many techniques for the removal of pollutants [8]. In the adsorption process, the nature of the adsorbent is fundamental to its feasibility and efficiency [9]. The design and manufacture of novel high-performance adsorbents, with greater adsorption capacity and longer service life, continue to be of research interest and technical challenge [10,11]. One approach in recent studies is to increase the number of functional groups for adsorption [12]. In view of the structural characteristics of phenolic contaminants, specifically the anionic phenolic hydroxyl groups and aromatic rings, multiple synergistic interfacial interactions (e.g. electrostatic attraction, π-π interaction, H-bonding, etc.) can be achieved by employing positively charged amines, aromatic-rings,

and/or oxygen-containing groups, on the adsorbent surface [13]. Another cost-effective way is to improve the accessibility (i.e. the utilization efficiency) of the engineered groups towards the contaminants [14]. For example, this might be done by constructing a specific geometry (such as a lamellar two-dimensional (2D) structure) of the adsorbents to increase the ratio of groups on the surfaces [15,16].

Among all the adsorbents trialed for the above purposes, engineered nano-materials (ENMs) have major potential [17,18], and porous organic polymers (POPs), in particular, have shown great promise in water remediation [19-21]. Supported by strong covalent bonds between light elements (C, N, B, O, H and so on), POPs possess great versatility in the number/type of chemical groups and pore structures, high surface area and structural stability [22-24]. Lamellar 2D ENMs, with well-designed structures, are able to combine the features of ENMs with the geometrical advantages of 2D materials. However, notwithstanding the above theoretical merits, most 2D ENMs, present non-negligible application limitations, including self-aggregation and inadequate recycling after use due to their nanoscale size [17,25]; such limitations reduce the treatment efficiency, increase the economic cost, and generate secondary environmental risks [26].

Integration of ENMs into macroscopic 3D porous carriers to construct novel hybrid adsorptive systems has been shown to be an approach that can overcome the above limitations and has considerable promise [27]. For example, the porous structure of carriers prevents self-aggregation of ENMs [28], and the facile collection and regeneration of the macroscopic adsorbents after use prevents the release of ENMs into the aquatic environment [29]. Based on the previous research by the authors and other researchers, polymeric ion exchangers are considered to be a suitable type of carrier for 2D ENMs in water remediation [26,30,31]. Such materials have abundant interconnected pores which provide accommodation for ENMs to tightly anchor on the

organic host substrate, due to the excellent compatibility between them. A reasonable selection of ion exchangers, such as some anion exchangers with numerous amino- and oxygen-containing groups, can aid the mass transfer and adsorption of phenolic compounds. With incorporation of 2D POPs into 3D ion exchangers, the geometrical features of the confined hierarchical pore structure in the 2D/3D hybrid adsorbents are believed to influence the adsorption performance [32]. However, as far as the authors are aware, the development of an adsorbent for organic contaminant removal in water treatment, by the integration of 2D POPs with 3D polymeric ion exchangers, has not been reported to-date.

In this paper, we demonstrate a successful proof-of-concept design and preparation of a novel adsorbent based on impregnating 2D POP (denoted as TCBD, formed with trimesoyl chloride (TC) as $C_3$ symmetric binding points and benzidine (BD) as $C_2$ links) into an inexpensive commercial 3D polyamine anion exchanger (D318) beads, *via* alternate deposition at room temperature. The integration of TCBD with D318 carrier in the preparation of a novel hybrid adsorbent (TCBD/D318), confers it with a remarkably greater water stability, more rapid solid-liquid separation after use, and enhanced anti-self-aggregation ability. The performance of the TCBD/D318 was evaluated systematically for the adsorption of four typical phenolic compounds (phenol, 1-naphthol, 4-nitrophenol and 4-chlorophenol) from water. High adsorption capacities, with improved atom economy, lower environmental sensitivity (to pH, coexisting inorganic salts and natural organic matter (NOM)), and reliable reusability, were demonstrated. The related interfacial adsorption mechanism was clarified by a combination of physico-chemical model fitting, instrumental analysis and chemical computation.

## 2. Experimental section

### 2.1 Materials

TC, BD, all four phenolic compounds (pH-dependences of species are shown in the Electronic Supplementary Information (ESI), Fig. S1), and humic acid (HA) were purchased from Sigma-Aldrich Inc. The D318 beads, provided by Jiangsu Jinkai Resin Industrial Co. Ltd, were selected for nanoparticles loading in this work for three reasons: (i) the polyamine groups of the D318 provide extra adsorption sites for anionic contaminants; (ii) the potential Donnan effect [33] exerted by the immobilized charged polyamine groups of D318 was expected to enhance permeation and pre-concentration of the target anion pollutants within the adsorbents; (iii) the polyamine groups in the D318 could act as anchor sites to fix TC units onto pore surfaces, for facilitating further TCBD growth on the surface in the repetitive deposition process. All other chemicals were bought from Sinopharm Chemical Reagent Co. Ltd. Water in all experiments was of ultrapure quality (18.2 $M\Omega \cdot cm^{-1}$).

### 2.2 Synthesis

Stock solutions A and B were prepared by dissolving TC (1.06 g) and BD (0.32 g), respectively, in ethyl acetate (30 mL). Solution B was added dropwise into solution A in a flask under magnetic stirring at 0$^{o}$C. The TCBD synthesis reaction, as illustrated in the ESI (Fig. S2), was allowed to proceed at 25$^{o}$C for 24 h. The resultant yellow solid powder (TCBD) was obtained after filtration, washing three times with water-ethanol solution (volume ratio of 1:1), and drying at 60$^{o}$C under vacuum. The basic characterization results of TCBD are given in the ESI (Text S1 and Fig. S3) to confirm the porous structure with designed functional groups.

The 2D/3D hybrid adsorbent TCBD/D318 was synthesized using a repetitive

deposition method, as depicted in Fig. 1. One cycle of the method comprised the following two steps: (1) D318 beads (1 g) (or all beads from the previous cycle) were soaked in solution A at 25°C under stirring for 20 min to anchor the $C_3$ symmetric binding points, and the beads were filtered out; (2) the beads was then soaked in solution B at 25°C under stirring for another 20 min, and filtered out. Dry weights of the beads were continuously recorded (ESI, Fig. S4) after each cycle, and reached a maximum value after six cycles. The final beads, with the maximum load of TCBD and the maximum adsorption capacity, were washed by a water-ethanol solution (volume ratio of 1:1), and dried at 60°C under vacuum.

**-Fig. 1-**

### 2.3 Batch adsorption and cyclic tests

Synthetic water was prepared by dissolving certain amounts of phenolic contaminants and other coexisting materials (inorganic salts, humic acid, and/or HCl (NaOH) solution to adjust pH) in water. Except for isothermal adsorption experiments, the initial concentration of phenolic contaminants was 100 mg/L. Adsorption tests were carried out in Erlenmeyer flasks shaken in air-bath incubators after the selected adsorbent (0.05 g in 100 mL) was added into each flask. The supernatant of the treated water was filtered by 0.45-μm membrane, diluted using glycine-HCl buffer solution (pH=2.3, to avoid pH effect on concentration determination), and then used to determine the contaminant concentration by UV absorption methods. The adsorption capacity ($Q_e$), as well as the isothermal and kinetic adsorption model parameters, were calculated using methods described in the ESI, Text S2.

After the equilibrium adsorption was reached, the TCBD/D318 beads were filtered from the flask, regenerated using 10 mL of water-ethanol solution (volume ratio of 1:1)

with HCl (pH=2) and $Na_2SO_4$ (0.5 wt.%), and washed using high purity water until the pH of the effluent reached 7. The beads obtained were then used for the next cycle.

### 2.4 Adsorbent characterization and chemical computation

Characterization of the adsorbents involved a range of techniques including the following: elemental composition analysis using a vario EL III elemental analyzer; morphological observations using a JEOL JEM-7600F scanning electron microscope (SEM) and a JEM-2100F transmission electron microscope (TEM); chemical structure using a Bruker Vector-22 Fourier transform infrared (FTIR) spectrometer, a Hitachi UH5300 UV-visible light spectrometer, a Rigaku D/max 2500VL/PCX-ray diffraction (XRD) spectrometer, and ESCALAB Xi+ X-ray photoelectron spectrometer (XPS); zeta potential (ZP) determination using a Malvern Nano-Z Zetasizer; and pore structure determination using a Micromeritics ASAP-2460 C automatic analyzer with $N_2$.

Gaussian 09 software was used for density functional theory (DFT) computations (using B3LYP hybrid function) of optimized spatial configurations of a typical fragment of the adsorbent and typical species of phenolic compounds, as well as pairwise complexes and corresponding binding energies (B.E. = $|E_{complex}-E_{TC/BD}-E_{contaminant}|$, where $E_{complex}$, $E_{TC/BD}$ and $E_{contaminant}$ were energies of the optimized geometry of a complex, the fragment of the adsorbent and the contaminant, respectively) between them. The fragment of the adsorbent contained one TC unit and one BD unit, by comprehensively considering computational cost and accuracy. The M06-2x/6-31+G(d) basis set method was employed to optimize all geometries [34-36].

## 3. Results and discussion

### 3.1 Characterizations of TCBD/D318

The TCBD/D318 adsorbent was designed according to the synthesis method summarized in Fig. 1. During the preparation the loading percentage of TCBD in the 2D/3D hybrid adsorbent, which is a basic parameter of nano-composites, was calculated using the dry weight of beads after every cycle of deposition (ESI, Fig. S4). The maximum loading was reached after six cycles, and the corresponding loading percentage was calculated to be ~22 wt.% using a weighing method. Since TCBD had much higher $Q_e$ for the four phenolic compounds than D318, as shown in the ESI (Fig. S5), a higher TCBD loading percentage was preferred. The TCBD content in the final TCBD/D318 after six cycles was also calculated using the elemental analysis method (ESI, Table S1 and Text S3), and a similar result (22.9 wt.%) was obtained.

The micromorphology of TCBD/D318 was observed by SEM and TEM (Fig. 2(a-d)). Compared to the SEM section image of D318, the image of TCBD/D318 showed many lamellar structures with curled edges, indicating the loading of 2D TCBD in the adsorbent. TEM images clearly demonstrated that nano-platelets of TCBD were present in the D318 matrix, and were well-distributed and without significant aggregation, which were features considered beneficial for contaminant adsorption.

**-Fig. 2-**

FTIR spectra (Fig. 2(e)) and XRD patterns (Fig. 1(f)) also revealed the incorporation of TCBD components in the final nanocomposite. In Fig. 2(e), peaks of TCBD/D318 at 1740 (end carboxyl groups), 1680 (amide I), 1620 (C=O conjugated with benzene rings), and 1587 $cm^{-1}$ (amide II), and within the fingerprint region (benzene rings), were characteristic vibration adsorption bands of TCBD. These oxygen- and nitrogen-containing groups, as well as aromatic rings, are all favored for binding interaction with phenolic compounds [13]. XRD patterns of TCBD/D318 showed a typical crystal structure of TCBD, which could provide a uniform distribution

of the above functional groups. The 2θ value of 6.56° indicated a crystal interplanar spacing of 13.5 Å (according to Bragg's law), consistent with the DFT calculated results of ~14 Å as shown in Fig. 1.

Isotherms of $N_2$ adsorption-desorption (Fig. 2(g)) showed that the specific area of the adsorbent beads after loading TCBD decreased from 20.33 to 16.62 $m^2/g$, whereas the average pore diameter increased from 17.33 to 27.51 nm. The inset figure of Fig. 2(g) illustrates the hierarchical pore structure in the 2D/3D hybrid adsorbent: after the deposition of TCBD, pores with diameters smaller than 10 nm were fewer due to the filling of TCBD nano-platelets; the decreased proportion of small pores increased the relative proportion of large pores. Such changes of pore size distribution engendered the decrease of surface area but the increase of average pore size.

The ZP-pH curves summarized in Fig. 2(h) exhibited another advantage of the nanocomposite over the 2D POP itself. While the TCBD was negatively charged at pH $\geq$ 6, the ZP of the TCBD/D318 was positive at all tested pH values (2-10), due to the polyamine structure of the D318 matrix. The relatively low sensitivity of the ZP to pH facilitates the application of TCBD/D318 over a wide range of pH conditions, especially in the case of treating the anionic species of phenolic contaminants at high pH values (ESI, Fig. S1).

### 3.2 Stability and solid-liquid separability

Two fundamental characteristics required of good nanomaterial-based adsorbents, especially in regard to industrial applications, are their stability and solid-liquid separability [18,37]. Since adsorbents can experience a wide pH range during the treatment of contaminated water and the regeneration process (contaminant desorption), their stability to variations in pH, is very important. To evaluate this, the TCBD and

TCBD/D318 were soaked in water at different pH values for 24 h, and the UV absorbance spectra of the water samples subsequently were determined, as shown in Fig. 3(a and b). The TCBD was not stable with changing pH, which was ascribed to the hydrolysis of amide bonds; the hydrolysis was clearly more marked under alkaline conditions. By comparison, after integration of the 2D TCBD into D318, the resulting nanocomposite exhibited outstanding water stability over the whole pH range (Fig. 3b). The 3D carrier notably prevented the POP from hydrolysis, which enables a longer life of the adsorbent and avoids secondary water pollution during use.

**-Fig. 3-**

In respect to the solid-liquid separability of the adsorbent, the tests showed that, after dispersal by shaking, the TCBD/D318 demonstrated a much faster gravity-driven separation from water (full separation after 10 seconds - see Fig. 3(d)) than TCBD (full separation after 10 hours - see Fig. 3(c)). This implied that the novel 2D/3D hybrid adsorbent could be used in a fully-mixed adsorption process with strong stirring, which can provide a considerably greater water treatment efficiency than a traditional column adsorption process. Furthermore, after settling the POP powder formed a hard cohesive layer that was difficult to re-disperse by shaking, whereas the TCBD/D318 layer could be easily re-dispersed. This would also facilitate the regeneration of the nanocomposite after use.

### 3.3 Adsorption behavior

#### 3.3.1 Effect of pH

The $Q_e$ values for the TCBD/D318 adsorbents with the four phenolic compounds, and at different pH values, are summarized in Fig. 4(a-d) (red lines). It can be seen that the nanocomposite exhibited a high $Q_e$ for all four contaminants at all pH values (Fig.

4 (a-d)) which was generally greater in comparison with the raw materials (D318 and TCBD), as can be seen in the ESI (Fig. S5). As one of the important aspects of the performance of adsorbents, $Q_e$ is affected by several operational parameters including the initial contaminant concentration and the adsorbent dosage. Comparison among different reported adsorbents for the adsorption of phenolic compounds in the ESI (Table S2) showed that, although not being the largest, the adsorption capacity of TCBD/D318 was at a relatively high level for each contaminant. Further comparison between the results given in Fig. 4(a-d) and in the ESI (Fig. S5) showed that, although TCBD had some similar (slightly lower) $Q_e$ values to TCBD and D318 at some pH values (for example pH 4, 6, or 8), the adsorption performance of the POP declined substantially at pH 2 and 10, when the POP itself was not stable, as shown in Fig. 3(a). In contrast, the performance of TCBD/D318 was less sensitive to pH and maintained a high level over the pH range. The reasons for this may be that in the low pH region, oxygen- and nitrogen-containing groups, and aromatic rings of the incorporated stable TCBD in D318 pores, could bind the contaminants through H-bonding and π-π interaction [38], while in the high pH region, the additional electrostatic attraction between the positively charged TCBD/D318 and phenolic anions further enhanced the adsorption, giving rise to an even greater performance.

**-Fig. 4-**

As the loading percentage of the TCBD component in the nanocomposite was ~22 wt.%, a theoretical physical quantity, referred to as the theoretical adsorption capacity (TAC), of the TCBD/D318, was proposed and calculated by simply summing the contribution of each part in the final adsorbent; thus, TAC = 22%×$Q_e$(TCBD) + 78%×$Q_e$(D318), where $Q_e$(TCBD) and $Q_e$(D318) were obtained from the data given in the ESI, Fig. S5. TAC values were plotted in Fig. 4(a-d) (dark green lines) in order to

illustrate the utilization efficiency of functional groups in the nanocomposite. It was evident that the experimentally derived $Q_e$ values were several times larger than the corresponding TAC. That is to say, the combination of TCBD with D318 generated a "synergistic" effect, which largely promoted the utilization efficiency (atom economy) of functional groups in the adsorption process. The synergistic effect, possibly resulting from the improved dispersibility of the POP in confined pores and the Donnan pre-concentration effect of polyamine groups of D318 [33], is a major advantage in terms of reducing the economic cost and undesired environment impacts of the adsorbent.

### 3.3.2 Effect of contaminant type

To understand in more detail the effect of contaminant type on adsorption, the values of $Q_e$ (mg/g) were converted to molar adsorption capacity (mmol/g) and their variation with pH are illustrated in Fig. 4(e). It was found that phenol, with the smallest molecular size (ESI, Fig. S1(a)), was the easiest to be adsorbed in most situations, except at pH 8 when phenol existed mainly as an undissociated (neutral) molecule, while 4-nitrophenol was substantially anionic (ESI Fig. S1(c)). The molar $q_e$ of 1-naphthol was the lowest among all four contaminants at most pH values, which may be due to the relatively larger size of one 1-naphthol molecule occupying a greater area of adsorption sites [39]. For 4-nitrophenol and 4-chlorophenol, which had similar molecular sizes, the greater adsorption of 4-nitrophenol may be attributed to the stronger electron-withdrawing effect of nitro groups, making 4-nitrophenol act as a stronger acid and π-electron acceptor, and binding more tightly with basic nitrogen-containing and π-electron donor groups in the nanocomposite, respectively.

### 3.3.3 Effects of coexisting anions

The adsorption of phenolic ions would be expected to be affected by the presence of other inorganic and organic anions due to their competitive effect. Therefore, the influence of widely existing anions in real water, both inorganic ($Cl^-$, $NO_3^-$ and $SO_4^{2-}$) and organic (HA), were studied. The results summarized in Fig. 5(a-d) illustrate the effects of inorganic anions on adsorption. Among the three competing inorganic ions, the degree of influence on $Q_e$ was in the following order: $SO_4^{2-}$ > $NO_3^-$ > $Cl^-$. The divalent anion $SO_4^{2-}$ had the relatively largest impact most likely because of its greater negative charge when competing with the phenolic compounds through electrostatic interaction with the TCBD/D318. While $NO_3^-$ and $Cl^-$ were equally mono-charged, the ability of the former to compete via H-bonding interaction meant that the impact of $NO_3^-$ was larger than that of $Cl^-$. However, notwithstanding these effects, it was evident that the adsorption performance of TCBD/D318 for all four phenolic contaminants was not substantially diminished by the presence of the inorganic anions, with only a slight decrease of adsorption capacities even at very high inorganic salt concentrations (~30 mmol/L). Thus, although the inorganic anions could compete in some forms of binding interaction between the adsorbent and contaminants (e.g. electrostatic), these appeared to be minor compared to other interaction(s), like π-π interaction, which enabled the uptake of phenolic compounds.

**-Fig. 5-**

The effect of HA, a widely used representative component of NOM in aquatic environments, on adsorption was studied at different concentrations and the results are shown in Fig. 5(e). Due to the structural similarities between HA and phenolic compounds, the HA could compete, in principle, through not only electrostatic attraction and H-bonding, but also π-π interactions. However, the results demonstrated that the adsorption performance for the phenolic compounds, with the exception of 1-

naphthol, was not significantly affected by the presence of HA. This behaviour suggested that, in addition to binding interactions, the adsorbent pore structure was another important factor that assisted in maintaining the adsorption performance. Thus, it is possible that the relatively large size of HA molecules were unable to enter the majority of pores of the TCBD/D318 [40], and thus could not occupy the adsorption sites; as 1-naphthol had the largest molecular size among the four contaminants, its uptake was therefore mostly affected.

### 3.4 Adsorption mechanism

Isothermal adsorption data (ESI, Fig. S6) were fitted by employing the Langmuir, Freundlich, and Redlich-Peterson models to investigate the interactions between TCBD/D318 and contaminants. The model fitting parameters are listed in the ESI, Table S3. Under most conditions, it was found that all three models had high regression coefficients ($R^2$), suggesting a mixed process of single- and multi-layer adsorption. The results further implied a multi-interaction-driven adsorption process [41], in which electrostatic attraction (single-layer), π-π interaction (multi-layer) and/or H-bonding (either single- or multi-layer) occurs [42].

The adsorption kinetic data were fitted to the pseudo first-order, pseudo second-order and intraparticle diffusion models. The comparison between pseudo first- and second-order models (ESI, Fig. S7 and Table S4) showed that the latter model described the data better with a higher $R^2$. This agreed with the chemical-interaction-driven process. Results obtained from the intraparticle diffusion model (ESI, Fig. S8 and Table S5) demonstrated a three-step process in total. Considering the pore-size distribution curves in the inset figure of Fig. 2(g), the first and fastest adsorption step was the diffusion of contaminants in macro- and meso-pores (> 2 nm) of TCBD/D318; the

second adsorption step was the diffusion in micropores (< 2 nm); and the last step was the equilibrium phase. The three steps confirmed the impact of the hierarchical pore structure on adsorption.

FTIR spectra of TCBD/D318 before and after loading phenolic compounds are illustrated in Fig. 6(a). Original N-H, O-H and amide I groups in TCBD/D318 all experienced a red-shift after adsorption (N-H and O-H: from 3466 to ~3423 $cm^{-1}$; amide I: from 1692 to 1660 $cm^{-1}$), indicating the formation of H-bonding between the adsorbent and phenolic contaminants [43]. C1s XPS spectra in Fig. 6(b-f) also detected C of phenyl C-O groups (marked in red colour) after adsorption, due to the phenyl groups adsorbed in the pores of the adsorbent. In addition, according to the normalized integral area percentages marked in Fig. 6(b-f), the significant decline of peak areas of C-C/C=C and C-N (except for 4-nitrophenol which had additional C-N) was attributed to the surface cover by the adsorbed phenolic contaminants.

**-Fig. 6-**

DFT computations directly displayed the optimized binding configuration as shown in Fig. 7. Here, the TCBD component was tested since it played a more dominant role in the adsorption than D318, as aforementioned. Obviously, π-π interaction and H-bonding took place at the same time for the adsorption. Furthermore, when adsorbed on to the same unit (either TC or BD) of the TCBD fragment, the anionic species of the contaminants had a larger B.E. than its neutral species (B.E. values in Fig. 7(b) > corresponding ones in Fig. 7(a); those in Fig. 7(d) > corresponding ones in Fig. 7(c)), which was evidence at a fundamental scale for the increasing $Q_e$ with increase of pH. Moreover, for the same species (either anionic or neutral) of phenolic contaminants, adsorption onto the TC unit had a larger B.E. than that onto the BD unit (B.E. values in Fig. 7(c) > corresponding ones in Fig. 7(a); those in Fig. 7(d) > corresponding ones in

Fig. 7(b)), which indicated that the contaminants preferred to be bound onto TC fragments. Such a phenomenon could be explained as follows: Since the two benzene rings of biphenyl structure in BD unit are twisted with a certain dihedral angle (Fig. 7(a and b)), π-π interactions between the contaminants and BD unit were inhibited due to steric hindrance, giving rise to the phenomenon that two phenyl ring planes in a BD-contaminant complex were not parallel to each other (Fig. 7(a and b)). Therefore, complexes formed by adsorption of contaminants onto BD unit had smaller B.E.

**-Fig. 7-**

Based on the above physico-chemical model fitting, instrumental analysis and chemical computation results, a schematic diagram of the adsorption of phenolic contaminants on TCBD/D318 was illustrated in Fig. 8 to clarify the multi-binding-interactions between the adsorbent and contaminants: (i) Polyamine groups on D318 skeleton with positive surface charges interacted with anionic phenolic compounds through electrostatic attraction; (ii) On the other hand, TCBD wielded more dominant binding interactions, including π-π interactions and H-bonding, in the adsorption of the contaminants.

**-Fig. 8-**

### 3.5 Reuse performance and storability

The capability of an adsorbent to be reused over many adsorption-desorption cycles without any notable loss in adsorption capacity ($Q_e$) is an important aspect that indicates whether it is economically favorable. Tests were undertaken to evaluate the reuse performance of TCBD/D318, and the results are summarized in Fig. 9(a). Of the four phenolic contaminants, the adsorption capacity for 4-nitrophenol was reduced the most after 10 cycles, which was attributed to it having the relatively strongest binding

interaction with the adsorbent, as discussed above and shown in Fig. 7. To identify the reason for the loss, changes in the pore structures and micromorphology of the adsorbent after regeneration/desorption were monitored. Fig. 9(b) shows a continuous decrease of specific surface area with the number of regeneration cycles, indicating some pores were blocked and could not be regenerated. On the other hand, the average pore diameter initially increased, but then decreased with further regeneration cycles. The increase in pore diameter after the first two cycles might result from the increased proportion of large pores after small pores were blocked, while the subsequent decline with further cycles was attributed to the accumulation of contaminants in large pores. SEM images of the adsorbent surface, illustrated in Fig. 9(c-g), suggested that, with the increase of cycle number, the large pores of the TCBD/D318 became visually smaller. Nevertheless, despite these observed changes and the discussion above regarding the fundamental reasons the reduction of $Q_e$, it should be noted that in practical terms, the TCBD/D318 exhibited an acceptable reusability for the adsorption of all four contaminants, with high $Q_e$ values maintained even after 10 cycles of use. In addition, recovery rates of the contaminants (recovery rate = desorbed contaminant amount of a certain cycle / adsorbed contaminant amount of the same cycle) in the desorption process over 10 cycles were measured (see the ESI, Fig. S9). It was found that, in all adsorption-desorption cycles except the first one, more than 94% of the adsorbed phenolic compounds in the adsorption process of a certain cycle could be desorbed and recovered in the desorption stage of the same cycle. Although treated as pollutants in water, the recovered phenolic compounds could also be used as valuable chemical raw materials in many industries, including the manufacture of dyes, pharmaceuticals, explosives, pesticides, phenolic resins, adhesives and so on [44,45]. Therefore, the high recovery rates of phenolic compounds from water can bring about not only notable

environmental benefits, but significant economic opportunities as well.

**-Fig. 9-**

Finally, the stability, or 'storability' of TCBD/D318 was tested. According to the comparison of adsorption capacities between freshly prepared TCBD/D318 and stored TCBD/D318 after six months (stored in the form of dried beads in the dark) as detailed in the ESI (Fig. S10), it was found that, except for the $Q_e$ loss of ~26% for 1-naphthol, which had the largest molecular size among four contaminants, the $Q_e$ loss for other three phenolic compounds was less than 8%, indicating good storability of the nanocomposite.

## 4. Conclusion

A new nanocomposite adsorbent, TCBD/D318, designed for the removal of phenolic compounds from water, was successfully fabricated by loading the 2D POP TCBD into pores of the carrier D318, via a facile repetitive deposition method at room temperature. TCBD/D318 exhibited a robust water stability over a wide pH range (2-12), a rapid solid-liquid separability (within 10 s) after dispersion in water, and a low tendency for self-aggregation. In addition to high adsorption capacities for four common phenolic contaminants (phenol, 1-naphthol, 4-nitrophenol and 4-chlorophenol), the TCBD/D318 adsorbent demonstrated a remarkably improved utilization efficiency of functional groups in the adsorption. The high adsorption performance was found to be largely insensitive to pH variation, and competition from the presence of coexisting inorganic salts and NOM (HA), due to the combined effects of multi-binding interactions and the hierarchical pore structure. Detailed study of the adsorption mechanisms showed that a hierarchical-pore-structure-induced multi-step diffusion adsorption process which was driven by multi-interactions, including

electrostatic attraction, π-π interactions, and H-bonding, and that contaminants were more inclined to be bound onto TC units of the TCBD in the nanocomposite. Finally, evidence for the reliable reusability and storability of TCBD/D318 was found. Overall, the results highlighted the great potential of TCBD/D318 for the removal of phenolic compounds from water, and suggested new opportunities for the environmental application of POP-based 2D/3D hybrid nanocomposites.


## Acknowledgements

The authors gratefully acknowledge the support of the following organizations: the National Natural Science Foundation of China (51978341), the Natural Science Foundation of Jiangsu Province of China (BK20190087), the China Scholarship Council (CSC), the National Major Project of Science and Technology Ministry of China (2017ZX07202-004), the Foundation of Jiangsu Collaborative Innovation Center of Biomedical Functional Materials, a project funded by the Priority Academic Program Development of Jiangsu Higher Education Institutions (PAPD), and the Scientific Computing Centre of NNU.


## References


[1] T.A. Larsen, S. Hoffmann, C. Luthi, B. Truffer, M. Maurer, Emerging solutions to the water challenges of an urbanizing world, Science 352 (2016) 51-59.

[2] Z.C. Li, L. Sellaoui, G.L. Dotto, A. Bonilla-Petriciolet, A.B. Lamine, Understanding the adsorption mechanism of phenol and 2-nitrophenol on a biopolymer-based biochar in single and binary systems via advanced modeling analysis, Chem. Eng. J. 371 (2019) 1-6.

[3] World Health Organization, International standards for drinking-water, (1958).

[4] Environmental Protection Agency, Methods 604. Phenols in federal register, 40 (1984) 136.

[5] Z. Hasan, S.H. Jhung, Removal of hazardous organics from water using metal-organic frameworks (MOFs): Plausible mechanisms for selective adsorptions, J. Hazard. Mater. 283

(2015) 329-339.

[6] Y. Pan, Y. Wang, A.M. Li, B. Xu, Q.M. Xian, C.D. Shuang, P. Shi, Q. Zhou, Detection, formation and occurrence of 13 new polar phenolic chlorinated and brominated disinfection byproducts in drinking water, Water Res. 112 (2017) 129-136.

[7] W.F. Young, H. Horth, R. Crane, T. Ogden, M. Arnott, Taste and odour threshold concentrations of potential potable water contaminants, Water Res. 30 (1996) 331-340.

[8] S. Lee, G. Barin, C.M. Ackerman, A. Muchenditsi, J. Xu, J.A. Reimer, S. Lutsenko, J.R. Long, C.J. Chang, Copper capture in a thioether-functionalized porous polymer applied to the detection of wilson's disease, J. Am. Chem. Soc. 138 (2016) 7603-7609.

[9] L. Meri-Bofi, S. Royuela, F. Zamora, M.L. Ruiz-Gonzalez, J.L. Segura, R. Munoz-Olivas, M.J. Mancheno, Thiol grafted imine-based covalent organic frameworks for water remediation through selective removal of Hg(II), J. Mater. Chem. A 5 (2017) 17973-17981.

[10] L.Q. Zhou, Z.J. Xu, K. Yi, Q.Y. Huang, K.G. Chai, Z.F. Tong, H.B. Ji, Efficient remediation of 2,4-dichlorophenol from aqueous solution using β-cyclodextrin-based submicron polymeric particles, Chem. Eng. J. 360 (2019) 531-541.

[11] N. Yao, X.T. Zhang, Z. Yang, W.B. Yang, Z.Q. Tian, L.M. Zhang, Norfloxacin and bisphenol-A eemoval using temperature-switchable graphene oxide, ACS Appl. Mater. Interfaces 10 (2018) 29083-29091.

[12] S.P. Zhang, Y.Y. Dong, Z. Yang, W.B. Yang, J.Q. Wu, C. Dong, Adsorption of pharmaceuticals on chitosan-based magnetic composite particles with core-brush topology, Chem. Eng. J. 304 (2016) 325-334.

[13] D.H. Lin, B.S. Xing, Adsorption of phenolic compounds by carbon nanotubes: Role of aromaticity and substitution of hydroxyl groups, Environ. Sci. Technol. 42 (2008) 7254-7259.

[14] Z. Yang, N. Zhuo, S.P. Zhang, Y.Y. Dong, X.T. Zhang, J.C. Shen, W.B. Yang, Y.P. Wang, J.Q. Chen, A pH- and temperature-responsive magnetic composite adsorbent for targeted removal of nonylphenol, ACS Appl. Mater. Interfaces 7 (2015) 24446-24457.

[15] H.J. Da, C.X. Yang, X.P. Yan, Cationic covalent organic nanosheets for rapid and selective capture of perrhenate: an analogue of radioactive pertechnetate from aqueous solution, Environ. Sci. Technol. 53 (2019) 5212-5220.

[16] Q. Sun, B. Aguila, L.D. Earl, C.W. Abney, L. Wojtas, P.K. Thallapally, S.Q. Ma, Covalent organic frameworks as a decorating platform for utilization and affinity enhancement of chelating sites for radionuclide sequestration, Adv. Mater. 30 (2018).

[17] T. Zhang, G.V. Lowry, N.L. Capiro, J.M. Chen, W. Chen, Y.S. Chen, D.D. Dionysiou, D.W. Elliott, S. Ghoshal, T. Hofmann, H. Hsu-Kim, J. Hughes, C.J. Jiang, G.B. Jiang, C.Y. Jing, M. Kavanaugh, Q.L. Li, S.J. Liu, J. Ma, B.C. Pan, T. Phenrat, X.L. Qu, X. Quan, N. Saleh, P.J. Vikesland, Q.Q. Wang, P. Westerhoff, M.S. Wong, T. Xia, B.S. Xing, B. Yan, L.L. Zhang, D.M. Zhou, P.J.J. Alvarez, In situ remediation of subsurface contamination: opportunities and challenges for nanotechnology and advanced materials, Environ. Sci. Nano 6 (2019) 1283-1302.

[18] Q.R. Zhang, Y. Han, L.C. Wu, Influence of electrostatic field on the adsorption of phenol on single-walled carbon nanotubes: A study by molecular dynamics simulation, Chem. Eng. J. 363 (2019) 278-284.

[19] Z.W. Liu, B.H. Han, Evaluation of an imidazolium-based porous organic polymer as radioactive waste scavenger, Environ. Sci. Technol. 54 (2020) 216-224.

[20] S.P. Zhang, Y.K. Li, C.H. Shi, F.Y. Guo, C.Z. He, Z. Cao, J. Hu, C.Z. Cui, H.L. Liu, Induced-fit adsorption of diol-based porous organic polymers for tetracycline removal, Chemosphere 212 (2018) 937-945.

[21] L.J. Huang, Q. Shuai, S.H. Hu, Tannin-based magnetic porous organic polymers as robust scavengers for methylene blue and lead ions, J. Clean. Prod. 215 (2019) 280-289.

[22] H.J. Ou, W.J. Zhang, X.F. Yang, Q.R. Cheng, G.Y. Liao, H. Xia, D.S. Wang, One-pot synthesis of g-C3N4-doped amine-rich porous organic polymer for chlorophenol removal, Environ. Sci. Nano, 5 (2018) 169-182.

[23] L.F. Zou, Y.J. Sun, S. Che, X.Y. Yang, X. Wang, M. Bosch, Q. Wang, H. Li, M. Smith, S. Yuan, Z. Perry, H.C. Zhou, Porous organic polymers for post-combustion carbon capture, Adv. Mater. 29 (2017) 1700229.

[24] Y.G. Zhang, S.N. Riduan, Functional porous organic polymers for heterogeneous catalysis, Chem. Soc. Rev. 41 (2012) 2083-2094.

[25] Z.H. Li, Y.Y. Liu, S.Y. Zou, C.B. Lu, H. Bai, H.B. Mu, J.Y. Duan, Removal and adsorption

mechanism of tetracycline and cefotaxime contaminants in water by $NiFe_2O_4$-COF-chitosan-terephthalaldehyde nanocomposites film, Chem. Eng. J. 382 (2020) 123008.

[26] S.J. Tesh, T.B. Scott, Nano-composites for water remediation: A review, Adv. Mater. 26 (2014) 6056-6068.

[27] C. Tian, J. Zhao, J. Zhang, S.Q. Chu, Z. Dang, Z. Lin, B.S. Xing, Enhanced removal of roxarsone by $Fe_3O_4$@3D graphene nanocomposites: synergistic adsorption and mechanism, Environ. Sci. Nano 4 (2017) 2134-2143.

[28] Z.W. Tong, D. Yang, J.F. Shi, Y.H. Nan, Y.Y. Sun, Z.Y. Jiang, Three-dimensional porous aerogel constructed by g-$C_3N_4$ andgGraphene oxide nanosheets with excellent visible-light photocatalytic performance, ACS Appl. Mater. Interfaces 7 (2015) 25693-25701.

[29] Q. Dong, J. Wang, X.G. Duan, X.Y. Tan, S.M. Liu, S.B. Wang, Self-assembly of 3D $MnO_2$/N-doped graphene hybrid aerogel for catalytic degradation of water pollutants: Structure-dependent activity, Chem. Eng. J. 369 (2019) 1049-1058.

[30] X.Z. Wang, N. Zhuo, C.G. Fu, Z.Q. Tian, H.G. Li, J.L. Zhang, W. Wu, Z. Yang, W.B. Yang, Enhanced selective adsorption of benzotriazole onto nanosized zeolitic imidazolate frameworks confined in polystyrene anion exchanger, Chem. Eng. J. 328 (2017) 816-824.

[31] X.L. Zhang, C. Cheng, J.S. Qian, Z.D. Lu, S.Y. Pan, B.C. Pan, Highly efficient water decontamination by using sub-10 nm FeOOH confined within millimeter-sized mesoporous polystyrene beads, Environ. Sci. Technol. 51 (2017) 9210-9218.

[32] Y. Xie, C.L. Chen, X.M. Ren, X.L. Tan, G. Song, D.Y. Chen, A. Alsaedi, T. Hayat, Coupling g-$C_3N_4$ nanosheets with metal-organic frameworks as 2D/3D composite for the synergetic removal of uranyl ions from aqueous solution, J. Colloid Interface Sci. 550 (2019) 117-127.

[33] Y.Y. Zhang, B.C. Pan, C. Shan, X. Gao, Enhanced phosphate removal by nanosized hydrated La(III) oxide confined in cross-linked polystyrene networks, Environ. Sci. Technol. 50 (2016) 1447-1454.

[34] H.S. Zhu, J.Y. Yuan, X.L. Tan, W.H. Zhang, M. Fang, X.K. Wang, Efficient removal of $Pb^{2+}$ by Tb-MOFs: identifying the adsorption mechanism through experimental and theoretical investigations, Environ. Sci. Nano 6 (2019) 261-272.

[35] W.J. Wang, J. Motuzas, X.S. Zhao, S.K. Bhatia, J.C.D. da Costa, Enhanced $CO_2$ sorption

efficiency in amine-functionalised 2D/3D graphene/silica hybrid sorbents, Chem. Commun. 54 (2018) 10586-10589.

[36] M.J. Frisch, G.W. Trucks, H.B. Schlegel, G.E. Scuseria, M.A. Robb, J.R. Cheeseman, G. Scalmani, V. Barone, B. Mennucci, G.A. Petersson, H. Nakatsuji, M. Caricato, X. Li, H.P. Hratchian, A.F. Izmaylov, J. Bloino, G. Zheng, J.L. Sonnenberg, M. Hada, M. Ehara, K. Toyota, R. Fukuda, J. Hasegawa, M. Ishida, T. Nakajima, Y. Honda, O. Kitao, H. Nakai, T. Vreven, J.A. Montgomery, Jr., J.E. Peralta, F. Ogliaro, M. Bearpark, J.J. Heyd, E. Brothers, K.N. Kudin, V.N. Staroverov, R. Kobayashi, J. Normand, K. Raghavachari, A. Rendell, J.C. Burant, S.S. Iyengar, J. Tomasi, M. Cossi, N. Rega, J.M. Millam, M. Klene, J.E. Knox, J.B. Cross, V. Bakken, C. Adamo, J. Jaramillo, R. Gomperts, R.E. Stratmann, O. Yazyev, A.J. Austin, R. Cammi, C. Pomelli, J.W. Ochterski, R.L. Martin, K. Morokuma, V.G. Zakrzewski, G.A. Voth, P. Salvador, J.J. Dannenberg, S. Dapprich, A.D. Daniels, Ö. Farkas, J.B. Foresman, J.V. Ortiz, J. Cioslowski, D. J. Fox, Gaussian 09, Revision E.01, Gaussian, Inc., Wallingford CT (2009).

[37] J. Lv, B. Wang, Y.B. Xie, P.L. Wang, L. Shu, X.O. Su, J.R. Li, Selective detection of two representative organic arsenic compounds in aqueous medium with metal-organic frameworks, Environ. Sci. Nano 6 (2019) 2759-2766.

[38] S.Y. Jia, Z. Yang, K.X. Ren, Z.Q. Tian, C. Dong, R.X. Ma, G. Yu, W.B. Yang, Removal of antibiotics from water in the coexistence of suspended particles and natural organic matters using amino-acid-modified-chitosan flocculants: A combined experimental and theoretical study, J. Hazard. Mater. 317 (2016) 593-601.

[39] J.C. Shen, X.Z. Wang, L.M. Zhang, Z. Yang, W.B. Yang, Z.Q. Tian, J.Q. Chen, T. Tao, Size-selective adsorption of methyl orange using a novel nano composite by encapsulating HKUST-1 in hyper-crosslinked polystyrene networks, J. Clean. Prod. 184 (2018) 949-958.

[40] X. Zhou, Y. Yang, C. Li, Z. Yang, W.B. Yang, Z.Q. Tian, L.M. Zhang, T. Tao, Environmental-friendly one-step fabrication of tertiary amine-functionalized adsorption resins for removal of benzophenone-4 from water, J. Clean. Prod. 203 (2018) 655-663.

[41] K. Vellingiri, Y.X. Deng, K.H. Kim, J.J. Jiang, T. Kim, J. Shang, W.S. Ahn, D. Kukkar, D.W. Boukhvalov, Amine-functionalized metal-organic frameworks and covalent organic polymers as potential sorbents for removal of formaldehyde in aqueous phase: Experimental versus

theoretical study, ACS Appl. Mater. Interfaces 11 (2019) 1426-1439.

[42] X.T. Zhang, J.C. Shen, N. Zhuo, Z.Q. Tian, P.R. Xu, Z. Yang, W. B. Yang, Interactions between antibiotics and graphene-based materials in water: A comparative experimental and theoretical investigation, ACS Appl. Mater. Interfaces 8 (2016) 24273-24280.

[43] Y.G. Peng, Y.X. Zhang, H.L. Huang, C.L. Zhong, Flexibility induced high-performance MOF-based adsorbent for nitroimidazole antibiotics capture, Chem. Eng. J. 333 (2018) 678-685.

[44] L.F. Ren, M. Adeel, J. Li, C. Xu, Z. Xu, X.F. Zhang, J.H. Shao, Y.L. He, Phenol separation from phenol-laden saline wastewater by membrane aromatic recovery system-like membrane contactor using superhydrophobic/organophilic electrospun PDMS/PMMA membrane, Water Res. 135 (2018) 31-43.

[45] M.L. Soto, A. Moure, H. Dominguez, J.C. Parajo, Recovery, concentration and purification of phenolic compounds by adsorption: A review, J. Food Eng. 105 (2011) 1-27.

## Captions

**Figure 1.** Schematic of TCBD/D318 synthesis.

**Figure 2.** (a and b) SEM and (c and d) TEM images of D318 and TCBD/D318; (e) FTIR spectra and (f) XRD patterns of different adsorbents; (g) $N_2$ adsorption–desorption isotherms of different adsorbents (inset: pore size distribution curves); (h) Zeta potential-pH curves of different adsorbents.

**Figure 3.** (a and b) UV spectra of water in which (a) TCBD or (b) TCBD/D318 was soaked for 24 h at different pH; (c and d) Gravity-driven solid-liquid separation of (c) TCBD and (d) TCBD/D318 in water.

**Figure 4.** (a-d) Experimental and theoretical adsorption capacities (TACs) of TCBD/D318 for different phenolic contaminants at different pH; (e) Molar adsorption capacities of TCBD/D318 for different phenolic contaminants at different pH.

**Figure 5.** Adsorption capacities of TCBD/D318 for different phenolic contaminants with the coexistence of (a-d) inorganic anions and (e) humic acid.

**Figure 6.** (a) FTIR and (b-f) C1s XPS spectra of TCBD/D318 before and after loading phenolic contaminants.

**Figure 7.** Optimized binding configurations and corresponding binding energies between TCBD fragments (adsorption onto (a and b) BD or (c and d) TC unit) and different species ((a and c) neutral and (b and d) anionic species) of phenolic compounds.

**Figure 8.** Schematic diagram of adsorption of phenolic contaminants on TCBD/D318.

**Figure 9.** Variation of (a) adsorption capacity (% initial capacity), (b) BET specific surface areas and average pore dimeters, and (c-g) micromorphology of TCBD/D318, over ten cycles of adsorption-desorption.

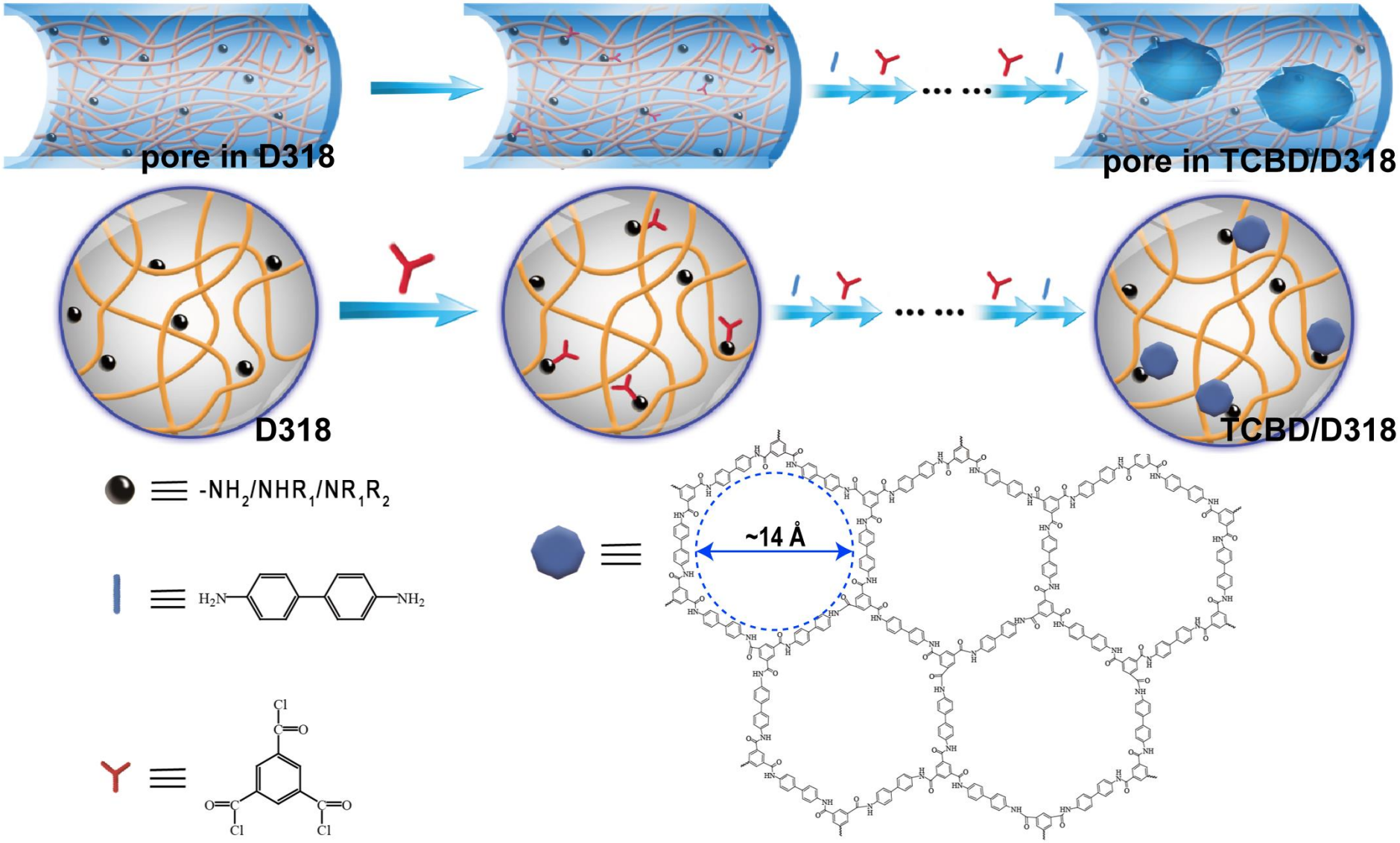


**Figure 1.** Schematic of TCBD/D318 synthesis.

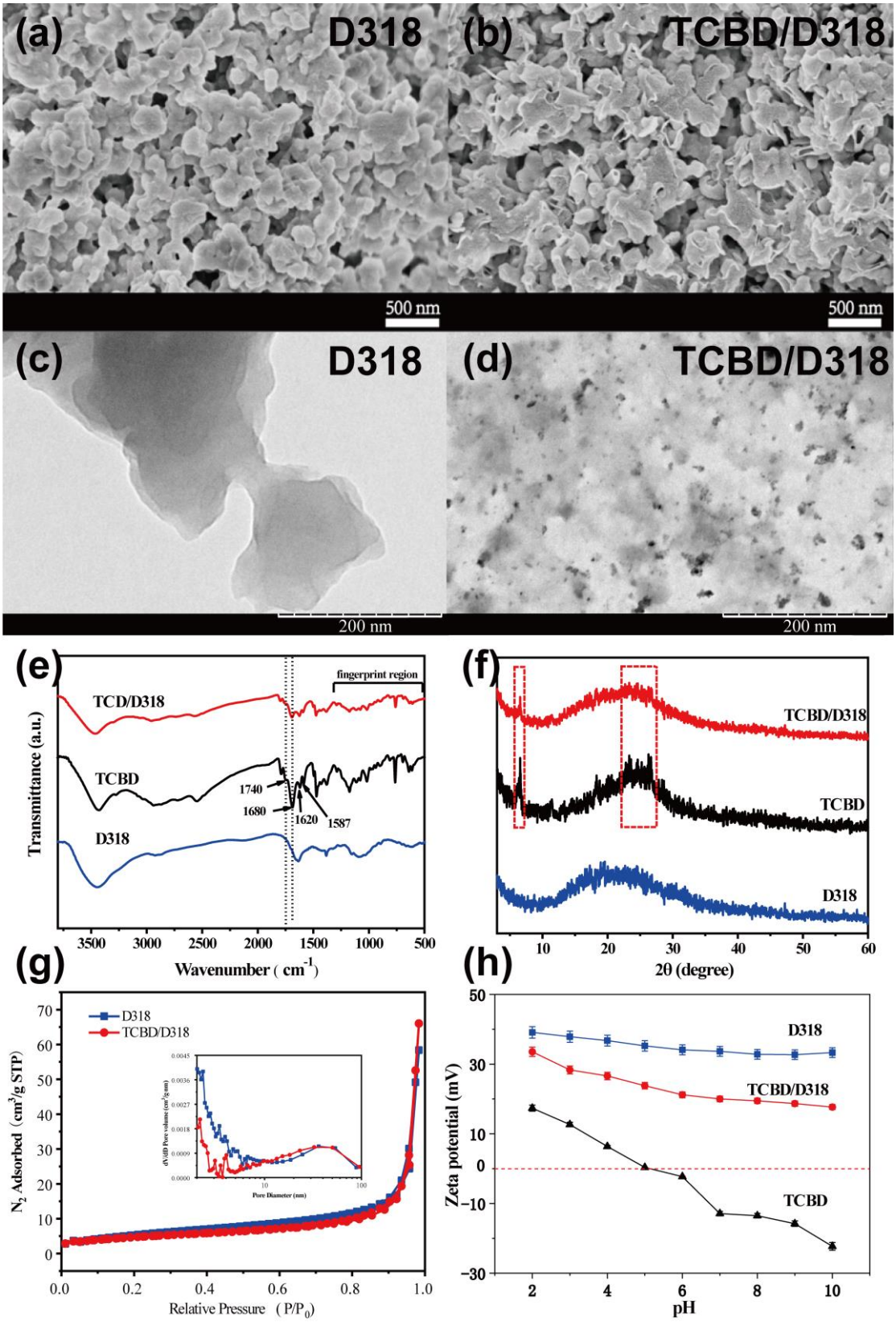


**Figure 2.** (a and b) SEM and (c and d) TEM images of D318 and TCBD/D318; (e) FTIR spectra and (f) XRD patterns of different adsorbents; (g) $N_2$ adsorption–desorption isotherms of different adsorbents (inset: pore size distribution curves); (h) Zeta potential-pH curves of different adsorbents.

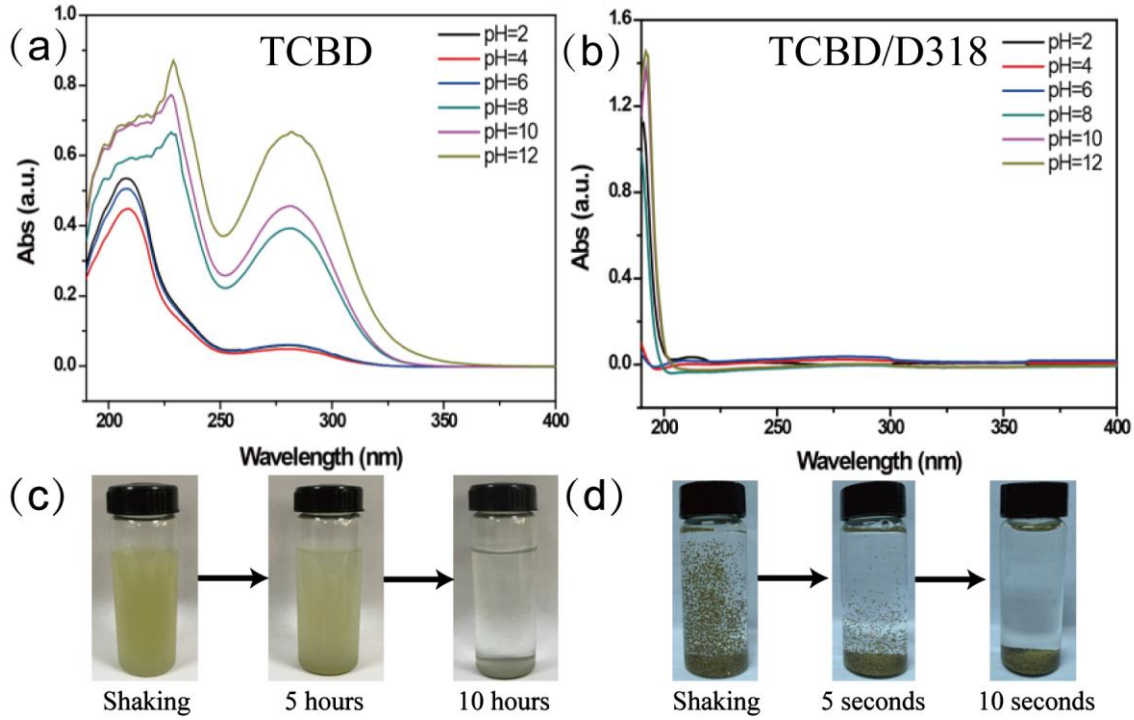


**Figure 3.** (a and b) UV spectra of water in which (a) TCBD or (b) TCBD/D318 was soaked for 24 h at different pH; (c and d) Gravity-driven solid-liquid separation of (c) TCBD and (d) TCBD/D318 in water.

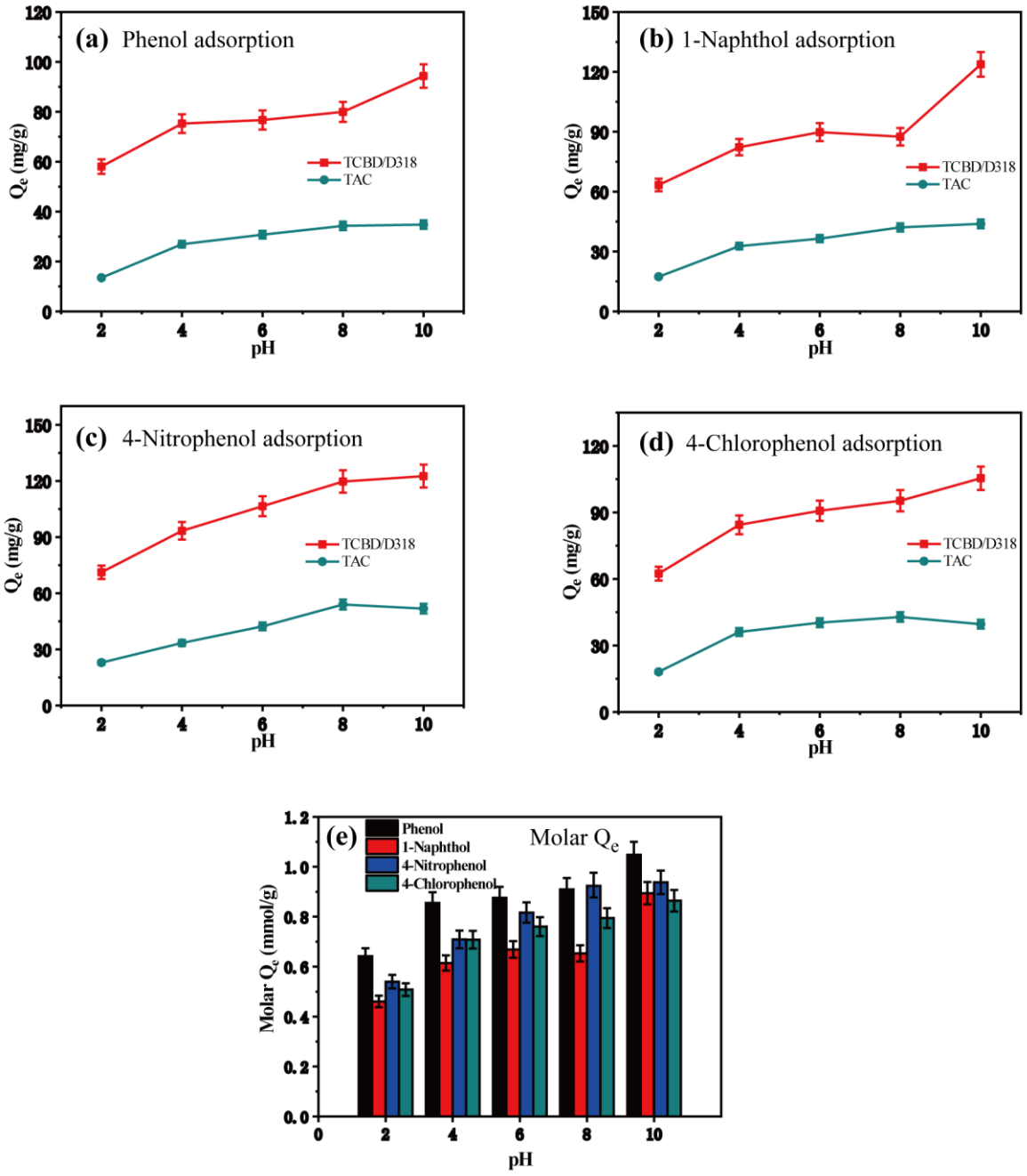


**Figure 4.** (a-d) Experimental and theoretical adsorption capacities (TACs) of TCBD/D318 for different phenolic contaminants at different pH; (e) Molar adsorption capacities of TCBD/D318 for different phenolic contaminants at different pH.

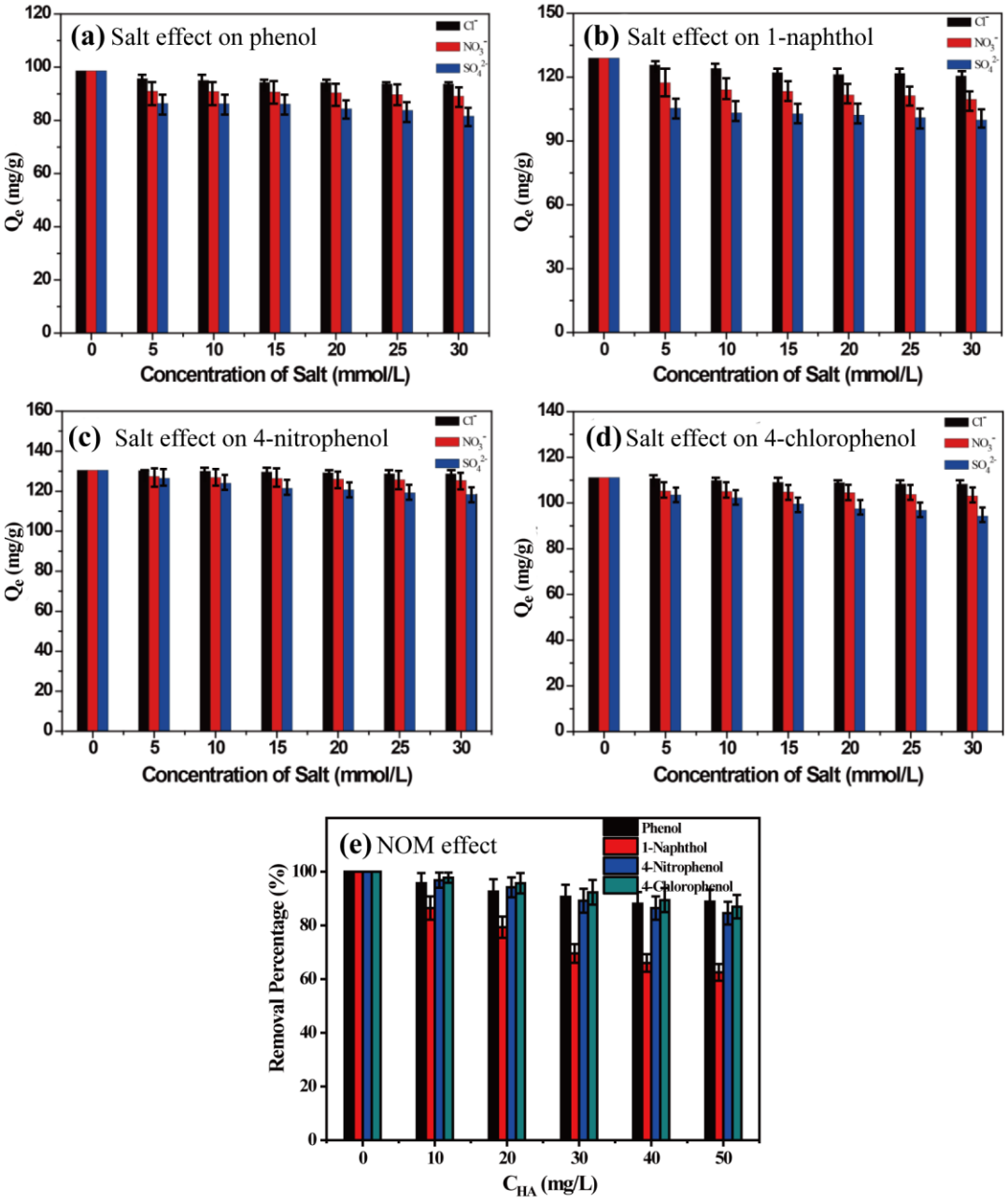


**Figure 5.** Adsorption capacities of TCBD/D318 for different phenolic contaminants with the coexistence of (a-d) inorganic anions and (e) humic acid.

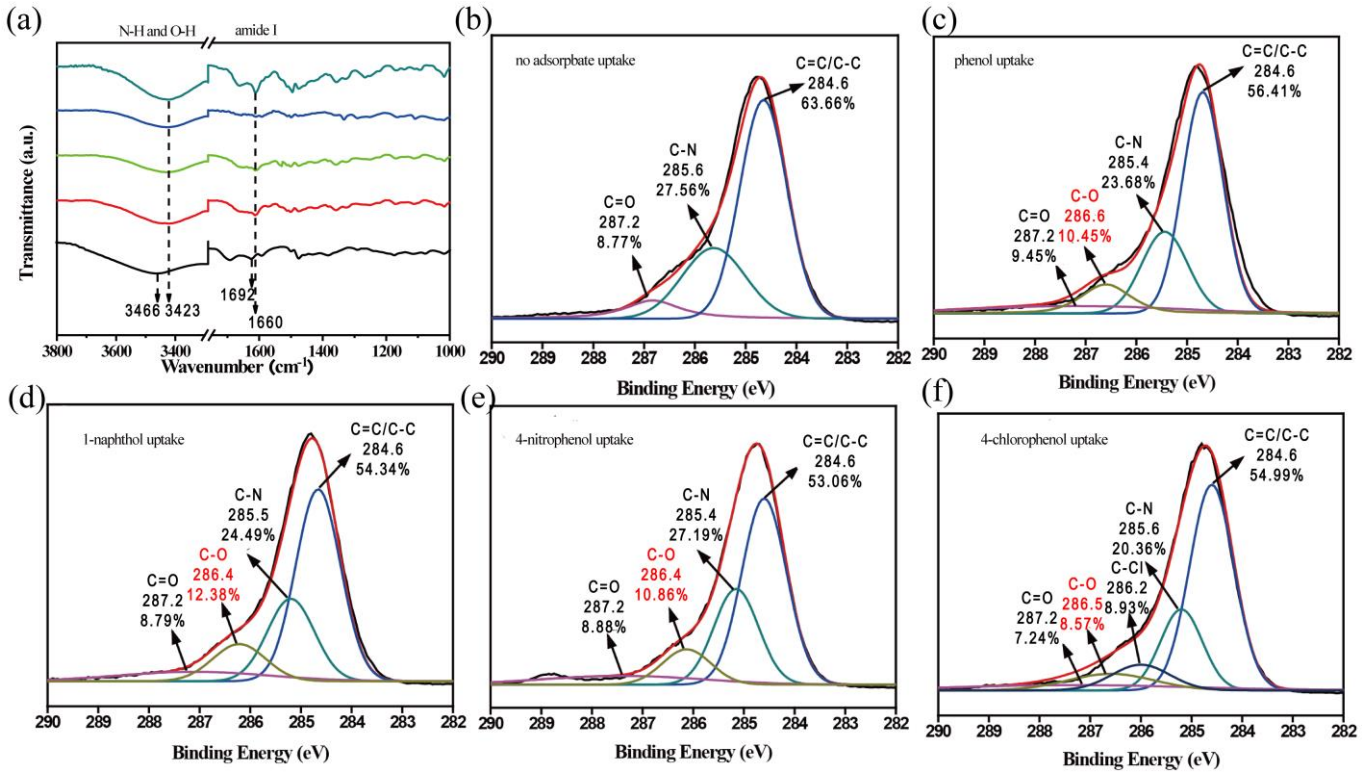


**Figure 6.** (a) FTIR and (b-f) C1s XPS spectra of TCBD/D318 before and after loading phenolic contaminants.

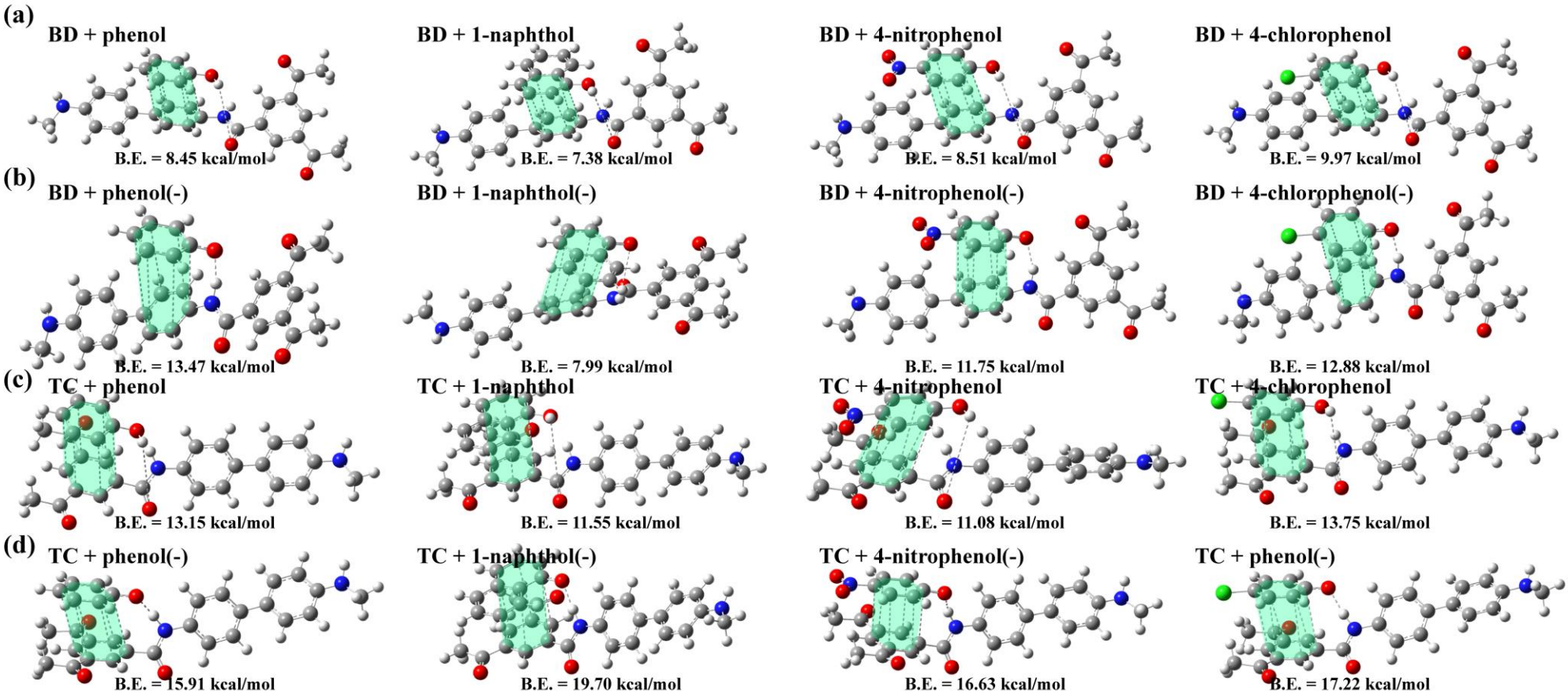


**Figure 7.** Optimized binding configurations and corresponding binding energies between TCBD fragments (adsorption onto (a and b) BD or (c and d) TC unit) and different species ((a and c) neutral and (b and d) anionic species) of phenolic compounds.

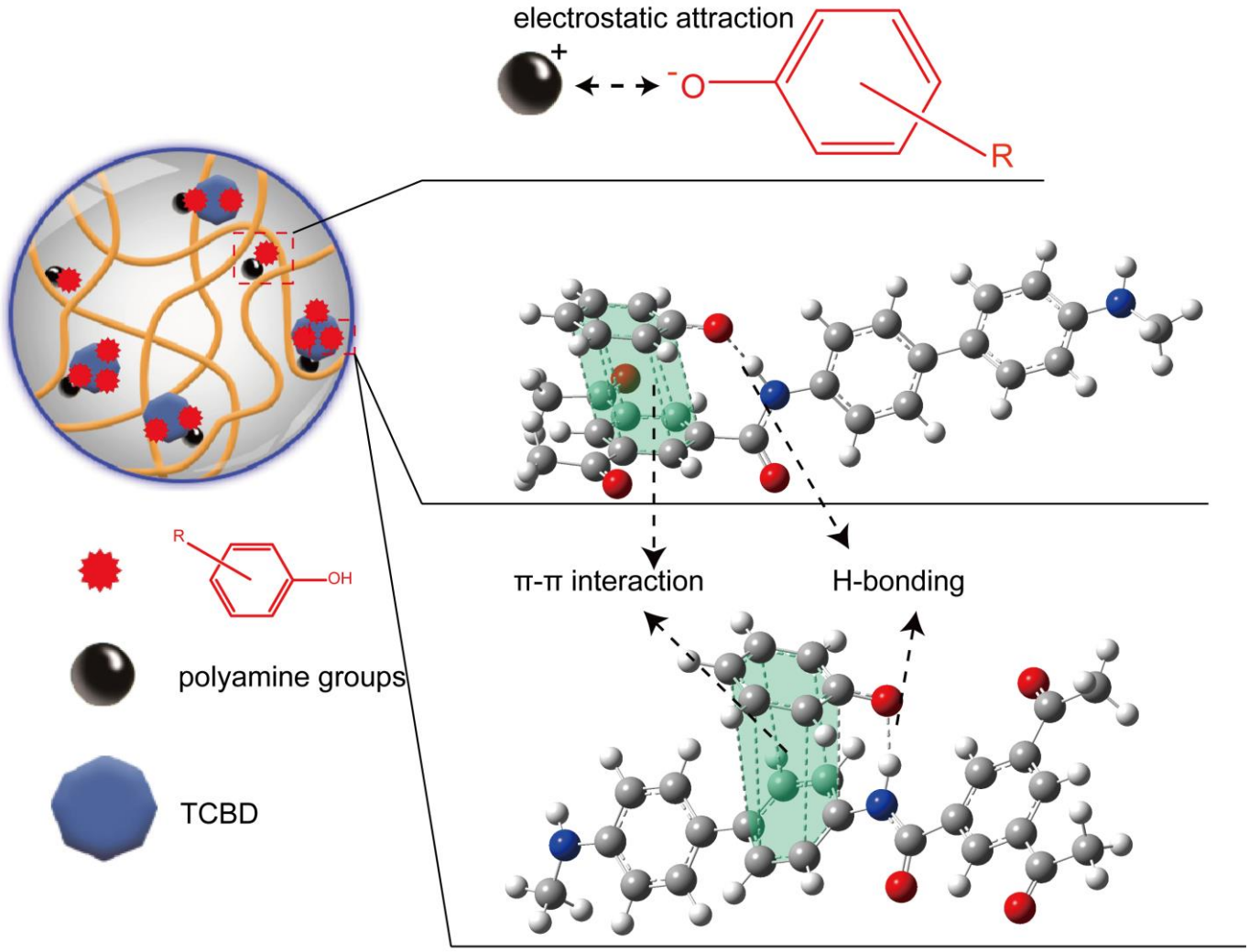


**Figure 8.** Schematic diagram of the adsorption of phenolic contaminants on TCBD/D318.

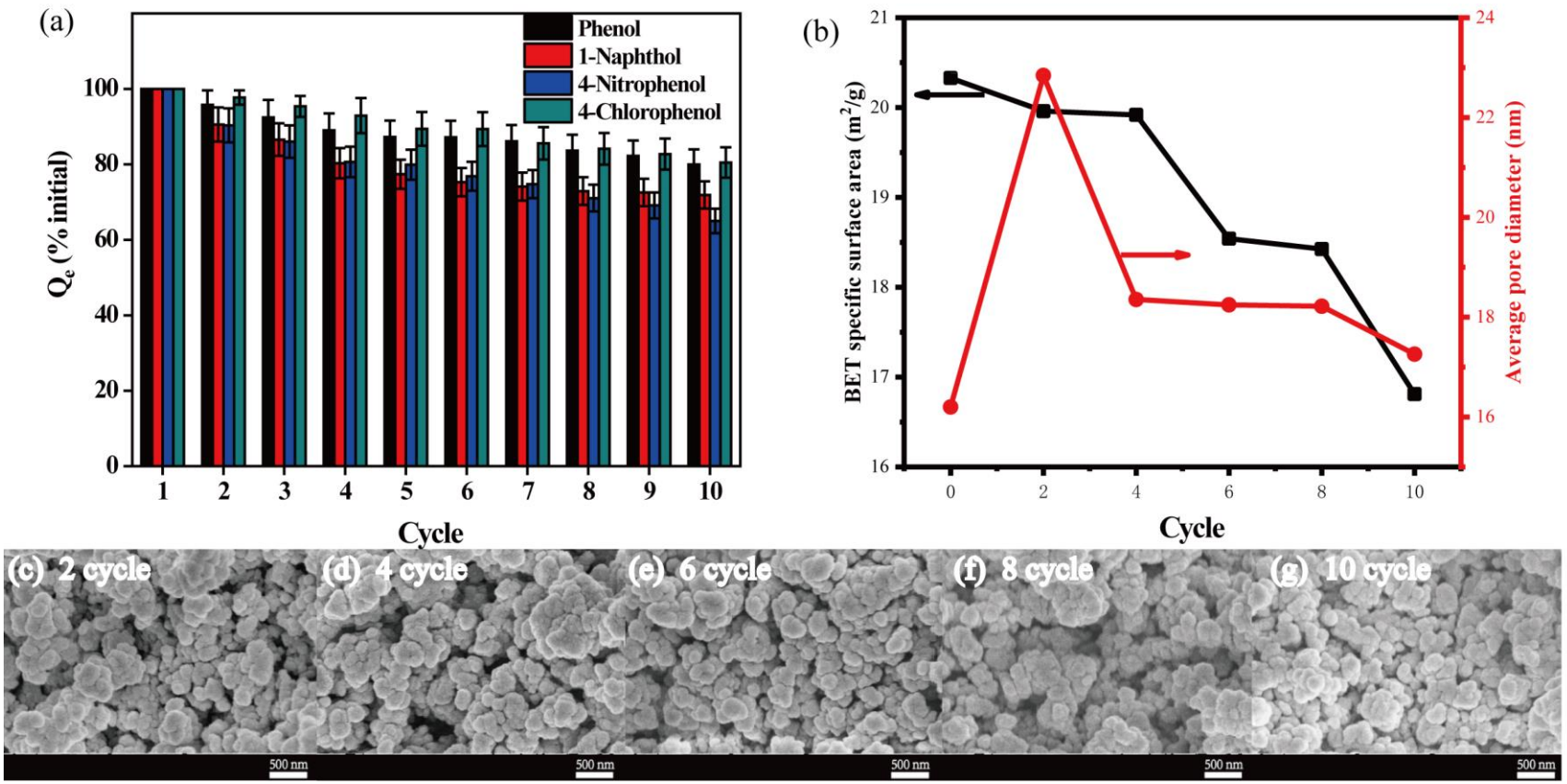


**Figure 9.** Variation of (a) adsorption capacity (% initial capacity), (b) BET specific surface areas and average pore dimeters, and (c-g) micromorphology of TCBD/D318, over ten cycles of adsorption-desorption.